03-FEBRUARY-1995 CB-NOTE XXX

Technical report of the $\pi^0\eta\eta$ analysis

Ralf Hackmann

Institut für Strahlen– und Kernphysik, Universität Bonn, D–53115 Bonn, Germany

Chapter 1

Preselection

The data for the analysis of the $\pi^0\eta\eta$ final state were taken from eight run periods using the zero–prong trigger. In addition we took data during october/november 1993 with a special software trigger in order to enhance the statistics of the $\pi^0\eta\eta$ final state.

Before kinematic fitting the data were subjected to a preselection which ensures a rather clean data–set of 6 PED–events. Several cuts were applied which are as listed (see also [?]);

- events with residual charged events were rejected.
- require exactly 6 PEDs
- cut events with PEDs in crystal type #13
- minimum energy of the central crystal has to be 10 MeV
- reject split–off events with the SMART–package [?]
- approximate energy–momentum conservation

$$1700\,\mathrm{MeV} < E_{tot} < 2050\,\mathrm{MeV} \qquad |\vec{p}_{tot}| \leq 100\,\mathrm{MeV}/c \tag{1.1}$$

Table 1.1 gives an overview of the data reduction for the zero–prong triggered data.

run period	December 1989	June 1990	July 1990	September 1990	November 1990	May 1991	June 1991	August 1991	$\sum$
zero–prong–events	1196452	1405733	4047615	1326536	4612529	1436770	1205406	1588655	16819696
neutral events	1091426	1266910	3603009	1145493	4137515	1245251	1066990	1386525	14943119
events with 6 PEDs	231574	268331	799228	236631	896870	266781	234287	233822	3167515
cut on type #13	188680	219098	681841	200617	772583	230689	201097	198872	2693477
central crystal energy >10 MeV	187180	146021	472133	196938	751170	228777	199526	177763	2359508
split–off–suppression SMART	174460	137608	447024	185484	708268	216223	188388	163911	2221366
approximate energy–momentum conservation	120600	101940	310313	140502	543672	169152	143703	124785	1654667

Table 1.1: *The result of the preselection using the zero–prong triggered data. After all cuts 9.8% of the whole data set remain.*

Chapter 2

Kinematic fitting

After the last step of the preselection the whole data set is fitted kinematically. For this purpose the standard program CBKFIT was used. The following hypotheses were fitted:

$$\begin{array}{lcll} \bar{\mathrm{p}}\mathrm{p} & \to & 6\gamma & (4\mathrm{C}) \\ \bar{\mathrm{p}}\mathrm{p} & \to & \pi^0\pi^0\pi^0 & (7\mathrm{C}) \\ \bar{\mathrm{p}}\mathrm{p} & \to & \pi^0\pi^0\eta & (7\mathrm{C}) \\ \bar{\mathrm{p}}\mathrm{p} & \to & \pi^0\eta\eta & (7\mathrm{C}) \\ \bar{\mathrm{p}}\mathrm{p} & \to & \eta\eta\eta & (7\mathrm{C}) \\ \bar{\mathrm{p}}\mathrm{p} & \to & \pi^0\pi^0\eta' & (7\mathrm{C}) \\ \bar{\mathrm{p}}\mathrm{p} & \to & \pi^0\eta\eta' & (7\mathrm{C}) \\ \bar{\mathrm{p}}\mathrm{p} & \to & \omega\omega & (8\mathrm{C}) \quad ,\omega \to \pi^0\gamma \end{array} \tag{2.1}$$

with any meson decaying into two photons:

$$\pi^0 \to \gamma\gamma, \quad \eta \to \gamma\gamma, \quad \eta' \to \gamma\gamma \tag{2.2}$$

The fit with respect to $\omega\omega$ is done by taking the decay mode $\omega \to \pi^0\gamma$ with $\pi^0 \to \gamma\gamma$ into account.

Due to the combinatorics of the 6γ final state one event can fit many hypotheses at once. Therefore an event is attributed to the hypothesis with the highest confidence level.

In order to speed up the kinematic fitting procedure some mass windows were set (see table 2.1). This means that events having an invariant $\gamma\gamma$–mass outside a mass windows were not passed to the kinematic fit.

To achive flat confidence level distribution and gaussian shaped pulls several error scalings were tried for the different run periods. The correction factors were set with the routine BCTTKS [?] and the TTKS–bank [?]. In table 2.2 the scaling factors which were used are listed.

Figure 2.1 shows the confidence level distribution for the hypotheses $\pi^0\eta\eta$ and figure 2.2 shows the pulls for the three kinematic quantities superimposed with a gaussian function. The gaussian function describes the distribution rather well with a standard deviation of ≈ 1 and a mean value of ≈ 0 except for $\sqrt{E}$. The exact values are given in table 2.3.

The $\gamma\gamma$ invariant mass spectrum is shown in figure 2.3 with 15 entries per event. One observes an apparent π^0–signal and η–signal. After rejecting those $\gamma\gamma$–combinations which combine to a π^0 or η the η' is clearly seen.

π^0:	135	$\pm$	65	MeV/c^2
η:	547	$\pm$	75	MeV/c^2
ω:	782	$\pm$	85	MeV/c^2
η':	958	$\pm$	100	MeV/c^2

Table 2.1: *Mass windows to preselect events for the kinematic fit*

run period	energy	θ	ϕ
December 1989	0.028	1.5	1.5
June 1990	0.028	1.6	1.6
July 1990	0.030	1.6	1.6
September 1990	0.028	1.3	1.3
November 1990	0.026	1.5	1.5
May 1991	0.026	1.6	1.4
June 1991	0.026	1.6	1.4
August 1991	0.028	1.7	1.5

Table 2.2: *Correction factors for the kinematic fit*

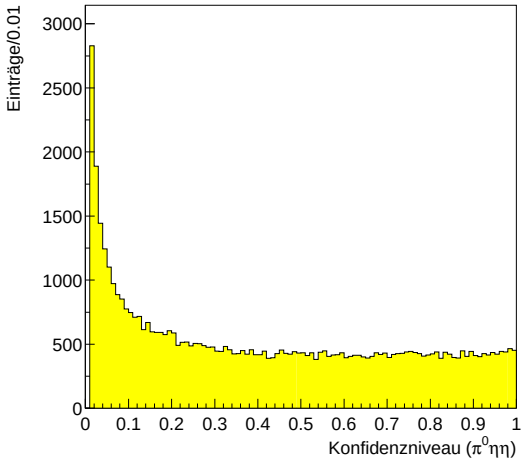

Figure 2.1:
Confidence level distribution for the hypotheses $\pi^0\eta\eta$

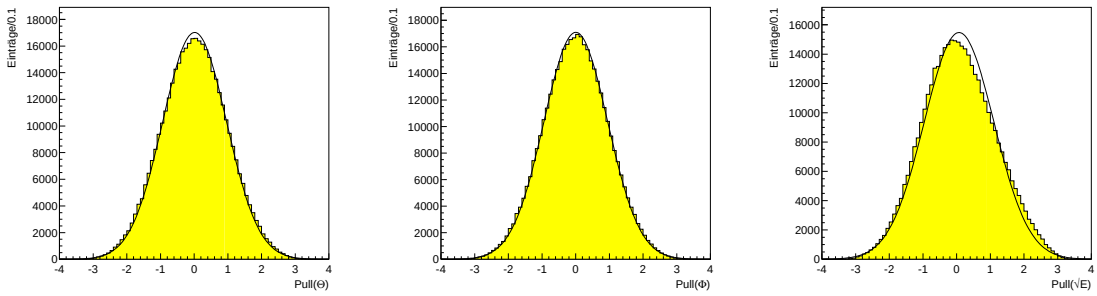

Figure 2.2: *Distribution of the pulls for the three kinematic quantities θ, ϕ and $\sqrt{E}$ for $\pi^0\eta\eta$*

	$\bar{x}_\theta$	σ_θ	$\bar{x}_\phi$	σ_ϕ	$\bar{x}_{\sqrt{E}}$	$\sigma_{\sqrt{E}}$
$\pi^0\eta\eta$	0.012	0.948	0.001	0.946	0.071	1.033

Table 2.3: *Mean and standard deviation of the pulls.*

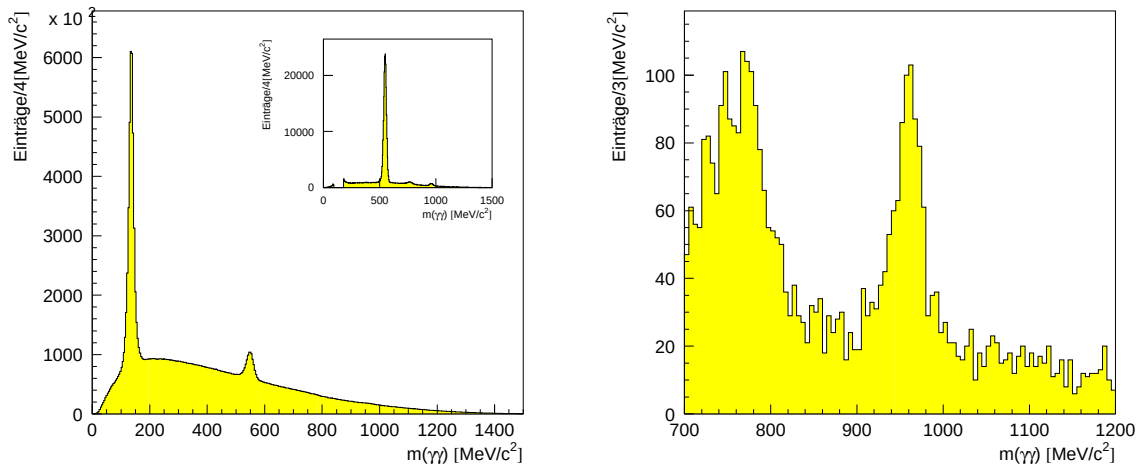

Figure 2.3: *$\gamma\gamma$–invariant mass spectrum (15 combinations per event). The right figure shows the η'–region after rejecting events which combine to a π^0 or to an η.*

In table 2.4 the number of events fitting each hypotheses are given were a 1%–cut in the confidence level distribution is applied.

hypothesis	#events
4C-Fit	1438046
$\pi^0\pi^0\pi^0$	839438
$\pi^0\pi^0\eta$	349712
$\pi^0\eta\eta$	53223
$\eta\eta\eta$	3929
$\pi^0\pi^0\eta'$	20779
$\pi^0\eta\eta'$	6150
$\omega\omega$	33594

Table 2.4: *Result of the kinematic fit*

The $\pi^0\pi^0\pi^0$ and $\pi^0\pi^0\eta$ final states are the strongest ones. The channel $\pi^0\eta\eta$ contributes with 30958 events after requiring a 10% confindence level cut as well as a 1%–veto to the competing hypotheses. The last cut is required in order to reduce background. In figure 2.4 shows the $\pi^0\eta\eta$ Dalitz plot of the untriggered data set.

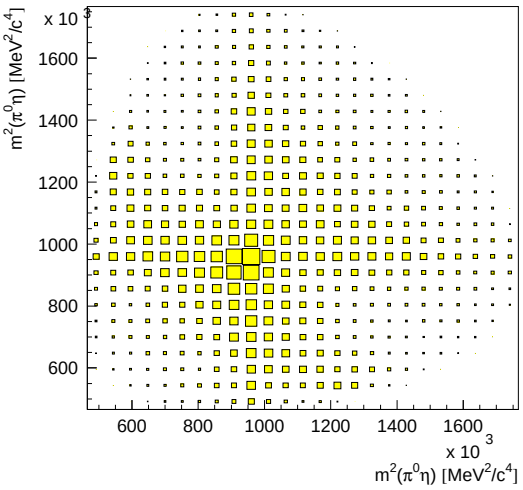

Figure 2.4:
Untriggered $\pi^0\eta\eta$–Dalitzplot

Chapter 3

Monte–Carlo–studies

In order to give an estimate of the expected background contribution, Monte–Carlo simulations of some potential background channels were done. These were some 5γ–, 6γ– and 7γ–final states. An event with five photons could be misidentified as a 6γ–event due to split–offs. A 7γ–event could contribute due to an undetected soft photon. In table 3.1 the channels which could contribute are listed.

generated final state	number of generated events
$\pi^0\pi^0\pi^0$	80000
$\pi^0\pi^0\eta$	80000
$\pi^0\eta\eta$	80000
$\eta\eta\eta$	80000
$\pi^0\eta\omega$	80000
$\pi^0\pi^0\omega$	80000
$\pi^0\omega$	60000
$\eta\omega$	80000
$\omega\omega$	80000

Table 3.1: *Overview of the generated Monte–Carlo–events*

The generated events passed the same analysis chain as real data The expected background contribution is given in table 3.2.

As expected the background due to 5γ channels does not contribute, because it is suppressed by SMART. The background to the $\pi^0\eta\eta$ channel is estimated to be $\approx 4.5\%$ and is dominated by the channel $\pi^0\pi^0\omega$. Despite the 1%–anticut the final state $\pi^0\pi^0\pi^0$ contributes with 0.8%. If one refused to apply the 1%–veto to the $\pi^0\eta\eta$ hypotheses, the number of events would increase to 41231, but at the expense of a background contamination of the order of 24%(!). This justifies the anticut. In figure 3.1 the distribution of the background events is shown. There is no special region of the phase space very strongly populated; it is rather flat.

	identified as $\pi^0\eta\eta$		
generated	MC–	true	relative
final state	events	events	contribution
$\pi^0\pi^0\pi^0$	8	244	$7.9 \cdot 10^{-3}$
$\pi^0\pi^0\eta$	13	166	$5.4 \cdot 10^{-3}$
$\pi^0\eta\omega$	205	230	$7.4 \cdot 10^{-3}$
$\pi^0\pi^0\omega$	86	720	$2.3 \cdot 10^{-2}$
$\pi^0\omega$	1	3	$1.0 \cdot 10^{-4}$
$\eta\omega$	2	5	$1.6 \cdot 10^{-4}$
$\omega\omega$	13	16	$5.1 \cdot 10^{-4}$

Table 3.2: *Expected background contribution*

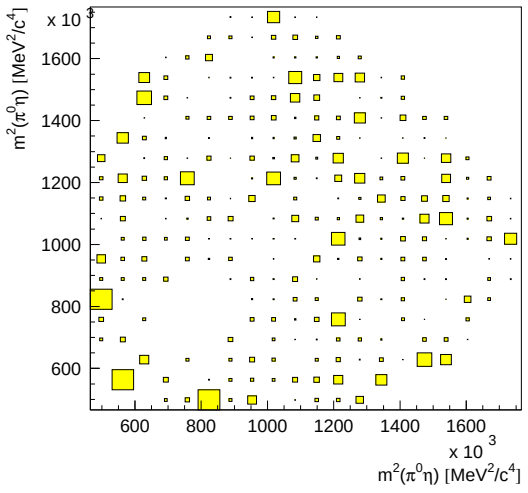

Figure 3.1:
Background distribution in the $\pi^0\eta\eta$ Dalitz plot

Chapter 4

Triggered data set

The triggered data were taken during October/November 1993 with the Software–trigger. The trigger is described in detail in [**?**].

The analysis chain for the triggered data was exactly the same as for the untriggered data. Table 4.1 gives the relevant numbers of the data reduction.

used triggered events	3256783
neutral events	3238648
events with 6PEDs	3027246
cut on type #13	2693818
central crystal energy $> 10\,\mathrm{MeV}$	2692930
split–off suppression SMART	2653898
Energy/momentum–cut	2433772
4C–fit with CL>1%	1997966
$\pi^0\eta\eta$ with CL>1%	281120
$\pi^0\eta\eta$ with CL>10% and anticut	166621

Table 4.1: *Data reduction of the triggered data set.*

The compatibility of the two $\pi^0\eta\eta$ data sets is verified using the χ^2 method (see also [**?**]). For both data sets a Dalitz plot was made consisting of 726 cells of magnitude $43360\,\mathrm{MeV}^2/c^4 \times 43360\,\mathrm{MeV}^2/c^4$. The χ^2 comparison took the different number of events of the two data sets into account. It resulted in χ^2=1.08 per cell. The difference of the triggered and the untriggered data set in terms of standard deviations (1σ) is shown in figure 4.1. A positive sign indicates a higher entry of the triggered data in comparison to the untriggered data and vice versa. The distribution does not exhibit distinct structures and all entries have a value of less than |3|. Therefore the two data sets are compatible and combined for further analysis. The $\pi^0\eta\eta$ Dalitz plot has now 197579 events.

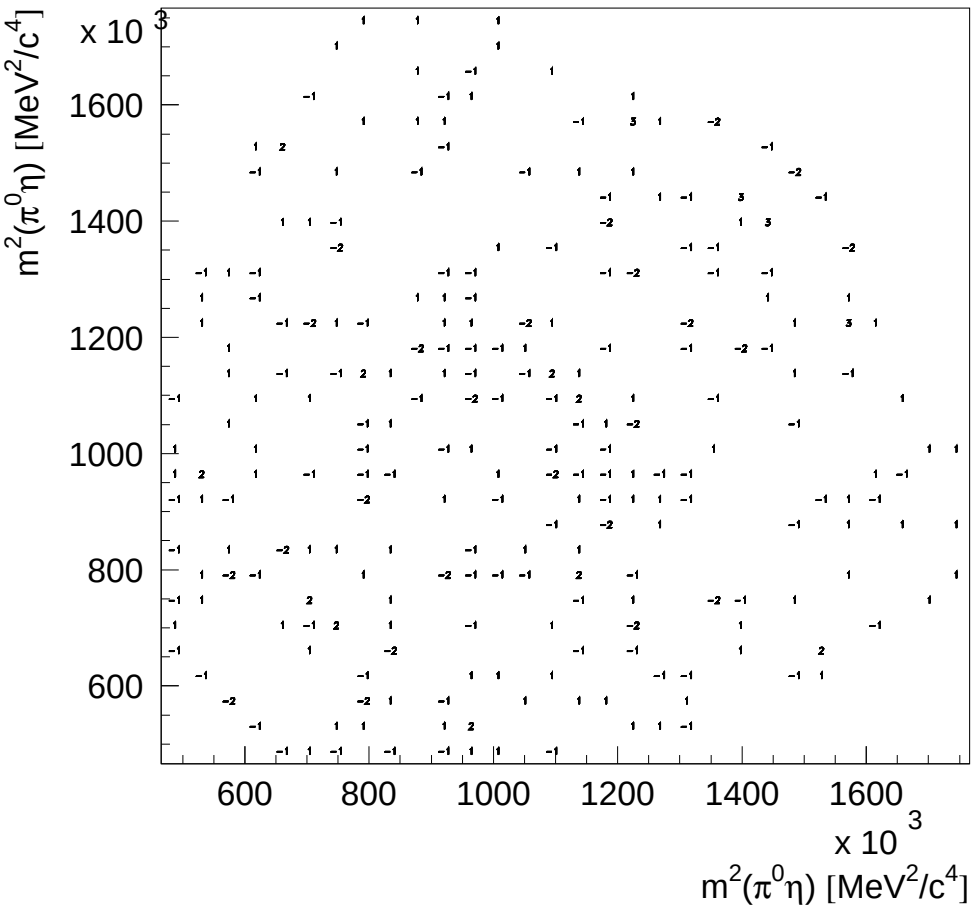

Figure 4.1: *Comparison between triggered and untriggered data The numbers give the difference of the two data sets in terms of the statistical error.*

Chapter 5

$\pi^0\eta\eta$–Dalitzplot

The possible initial states from which the annihilation can take place are given in table 5.1. Only initial states and intermediate resonances with angular momentum less equal 2 are taken into account. This leaves the three possibilities $^1S_0$, $^3P_1$ and $^3P_2$.

inital state				decay into			
$^{(2I+1)(2S+1)}L_J$	$I^G(J^{PC})$	L	ℓ	$\pi^0\eta$	$\eta\eta$	$Z_{J^{PC},L,\ell}(\vec{P},\vec{Q})$	angular distribution
$^{31}S_0$	$1^-(0^{-+})$	0	0	$\times$	$\times$	$\mathbb{1}$	1
		1	1	$\times$		$\vec{Q}\cdot\vec{P}$	$\cos^2\theta$
		2	2	$\times$	$\times$	$(\vec{Q}\cdot\vec{P})^2-\frac{1}{3}\lvert\vec{Q}\rvert^2\lvert\vec{P}\rvert^2$	$(\cos^2\theta-\frac{1}{3})^2$
$^{33}P_1$	$1^-(1^{++})$	1	0	$\times$	$\times$	$\vec{P}$	1
		0	1	$\times$		$\vec{Q}$	1
		1	2	$\times$	$\times$	$\vec{Q}(\vec{Q}\cdot\vec{P})-\frac{1}{3}\lvert\vec{Q}\rvert^2\vec{P}$	$\cos^2\theta+\frac{1}{3}$
		2	1	$\times$		$\vec{P}(\vec{P}\cdot\vec{Q})-\frac{1}{3}\lvert\vec{P}\rvert^2\vec{Q}$	$\cos^2\theta+\frac{1}{3}$
$^{33}P_2$	$1^-(2^{++})$	1	2	$\times$	$\times$	$\vec{Q}\bigotimes(\vec{Q}\wedge\vec{P})+(\vec{Q}\wedge\vec{P})\bigotimes\vec{Q}$	$\sin^2\theta$
		2	1	$\times$		$\vec{P}\bigotimes(\vec{P}\wedge\vec{Q})+(\vec{P}\wedge\vec{Q})\bigotimes\vec{P}$	$\sin^2\theta$

Table 5.1: *Allowed inital and final angular momentum states and angular distributions with the restriction of* $\ell+L\leq 4$.

Figure 5.1 shows the $\pi^0\eta\eta$–Dalitzplot of the combined dataset. The main characteristics are well known. Clearly visible is a cross like structure at a $\pi^0\eta$ invariant mass around 1 GeV due to the $a_0(980)$. Further intensity is observed in two bands at an $\eta\eta$ invariant mass at approximate 1350 MeV and 1500 MeV.

The fit of the theoretical amplitude to the experimentel distribution is done using the χ^2–method. The Dalitzplot contains 2×1798 active cells each having a size of $18523\,\mathrm{MeV}^2/c^4\times 18523\,\mathrm{MeV}^2/c^4$. The total number of entries is 2×197579 with the maximum number of entries of 416 and the minimum number of entries of 19 events.

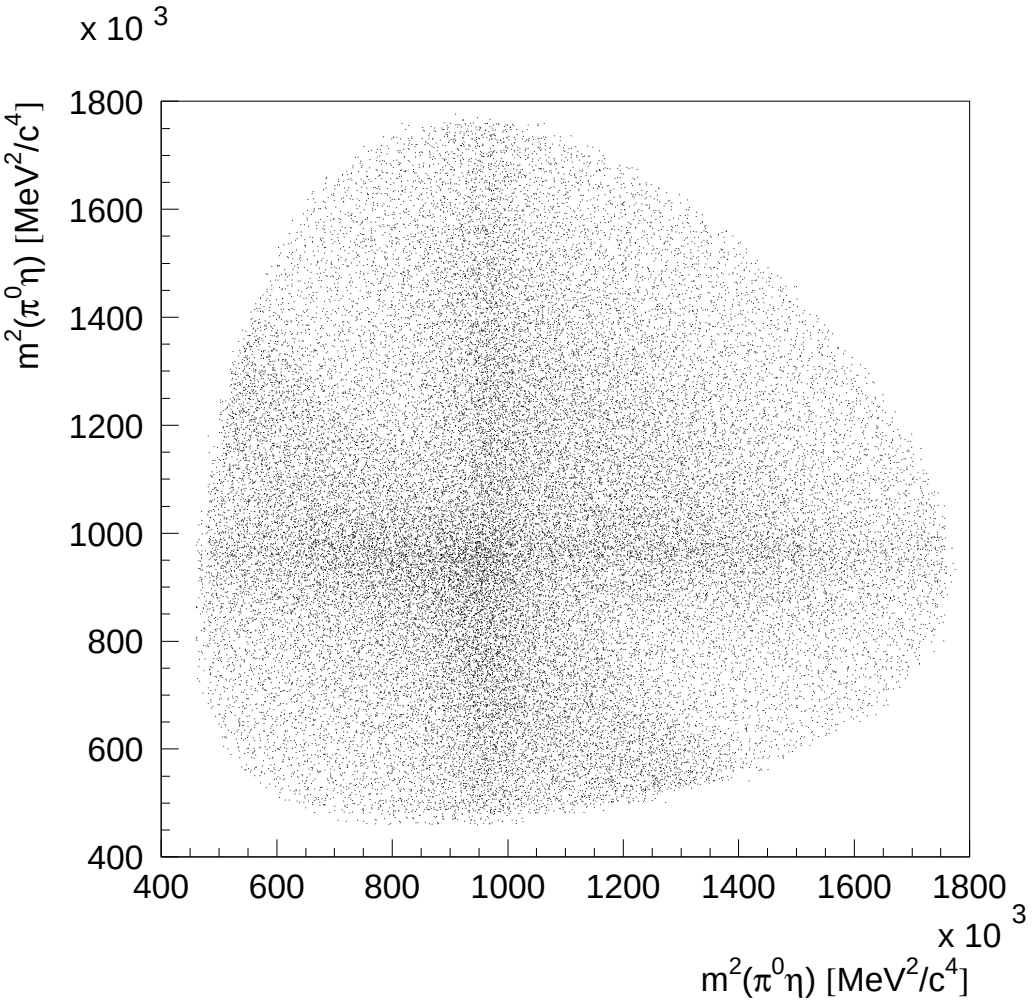

Figure 5.1: $\pi^0\eta\eta$–*Dalitzplot of the combined data set.*

Chapter 6

Acceptance correction

In order to check the acceptance 400000 phase space distributed Monte–Carlo events were generated which were subjected to the same analysis chain as real data. In figure 6.1 the MC–event distribution is shown. the acceptance has a maximum in the center of the Dalitzplot and decreases in the direction of the phase space boundary. The maximum is 29.3% and the minimum is at 24%. To correct the data, the distribution is fitted using the angular distribution functions. The fit is then normalized in a manner, so that each cells provides a correction factor which is multiplied to the Dalitzplot entry.

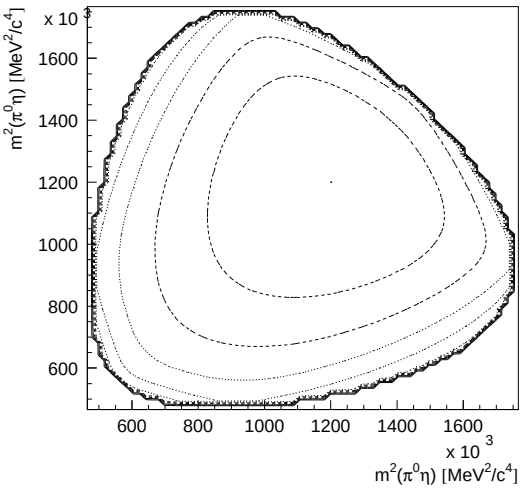

Figure 6.1:
Acceptance distribution

Chapter 7

Partial wave analysis

The partial wave analysis of the $\pi^0\eta\eta$–Dalitzplot is carried out using the K–matrix formalism [?]. In order to figure out the masses, widths and the contribution of the intermediate resonances to the Dalitzplot about 200 fits were made. A list of some characteristic fits is given in table A.1. Table A.2 gives the corresponding K–matrix poles and table A.3 the complex production strength for the $^1S_0$–initial state. The T–matrix poles are listed in table A.4 and table A.5 gives the contribution of the poles. The final result is given in table 7.6 where the medians for the resonance parameters are derived from a series of fits. In the following the general behaviour of the fits is outlined:
The analysis of the $\pi^0\eta\eta$ final state uses the parametrization of the $\pi^0\eta$–S–wave from the $\pi^0\pi^0\eta$–analysis [?]. There the $\pi\pi$–scattering data were used in order to fix the $\pi\pi$ interaction and to determine the $\pi^0\eta$ interaction. Here the main aim was a determination of the $\eta\eta$ interaction.

#	$a_0(980)$ $^1S_0$			$\eta\eta$–S–wave $^1S_0$				$\eta\eta$–2^{++}–BW		$a_2(1320)$ fix	χ^2/N_{dof}	P/S
	BW	$\pi^0\eta$–S–wave fix	$\pi^0\eta$–S–wave free	1×1	2×2 $\eta\eta/\eta\eta'$	2 Poles	3 Poles	$^1S_0$	S+P	S+P		
1	x			x			x		x		1.33	0.27
2	x				x		x		x		1.33	0.27
3			x	x		x			x		1.29	0.00
4			x	x			x		x		1.23	0.00
5			x		x		x		x		1.23	0.00
6		x		x			x		x		1.42	0.15
7		x			x		x		x		1.42	0.15
8	x			x			x		x	x	1.27	0.29
9		x		x			x		x	x	1.23	0.20
10		x		x			x	x			1.44	0.00

Table 7.1: *The table gives the hypotheses tried to fit the data.*

- The starting point of the analysis is fit #6 with a fixed $\pi^0\eta$ parametrization. The $\eta\eta$–S–wave was parametrized as a 1×1–K–matrix with 3 poles. The continuous rise

Fit–#	$\eta\eta$–S–wave poles								
	m_1	$\widetilde{\Gamma}_{11}$	$\widetilde{\Gamma}_{12}$	m_2	$\widetilde{\Gamma}_{21}$	$\widetilde{\Gamma}_{22}$	m_3	$\widetilde{\Gamma}_{31}$	$\widetilde{\Gamma}_{32}$
1	1358	183	–	1562	158	–	$1.7 \cdot 10^5$	19	–
2	1359	181	–	1563	158	3.4	$1.4 \cdot 10^5$	23	–
3	1309	267	–	1548	172	–	–	–	–
4	1341	175	–	1547	143	–	$1.3 \cdot 10^5$	23	–
5	1341	175	–	1546	143	0.2	$1.3 \cdot 10^5$	22	–
6	1317	181	–	1514	104	–	$1.3 \cdot 10^5$	22	–
7	1317	181	–	1514	104	15	$1.2 \cdot 10^6$	20	–
8	1371	172	–	1570	156	–	$1.7 \cdot 10^5$	19	–
9	1352	121	–	1567	187	–	$1.3 \cdot 10^5$	21	–
10	1337	172	–	1548	144	–	$1.3 \cdot 10^5$	23	–

Table 7.2: *The K–matrix poles of $\eta\eta$–S–wave*

of the $\eta\eta$–S–wave beyond the phase space limit is parametrized by the third pole. Further an $\eta\eta$ tensor contribution is needed (BW–amplitude). In contrast to the S–waves the D–wave is allowed from S– as well as P–initial states. The fit converged at $\chi^2/\mathrm{N_{dof}}$=2528/(1798-21)=1.42.

- The necessity of the tensor contribution is checked by a fit omitting the 2^{++} amplitude from fit #6. This resulted in an increase of χ^2 by $\Delta\chi^2$=+609. Figure 7.1 shows the deficiencies of the description without the tensor.

- A restriction to the S initial state only is done with fit #10. The change in χ^2 in comparison to fit #6 is only $\Delta\chi^2$=+43. But here the 2^{++} resonance is rather narrow with $\Gamma = 48\,\mathrm{MeV}/c^2$.

- In fits #3, #4 and #5 the poles of the $\pi^0\eta$–S–wave were released. In general this improves the fit. It has some interesting effects. First of all the contribution from P initial states is completely removed. Further the contribution of the $\pi^0\eta$–S–wave is at maximum for these fits. The T–matrix poles indicate a rather broad $a_0(980)$ with a width of the order of $300 \ldots 400\,\mathrm{MeV}/c^2$.

- The first analysis of $\pi^0\eta\eta$ [**?**] used only two poles for the $\eta\eta$–S–wave. So a canonical ansatz would be a K–matrix with 2 poles. But this attempt failed. The χ^2 increased by $\Delta\chi^2$=+344 in comparison to fit #6. In fit #3 the 2–pole solution is given but with a released $\pi^0\eta$–S–wave. Therefore the 3–pole solution is further investigated.

- In fits #1, #2 and #8 the $\pi^0\eta$–parametrization is substituted by a Breit–Wigner amplitude. Mass and width for the $a_0(980)$ are $(m, \Gamma) = (982, 52)\,\mathrm{MeV}/c^2$ for each fit. Interestingly the introduction of the Breit–Wigner parametrization for the $a_0(980)$ leads to an exchange of the masses of the $\eta\eta$–S–wave pole around $1500\,\mathrm{MeV}/c^2$ and the 2^{++}–$\eta\eta$–resonance.

- The use of a second coupling for the $1500\,\mathrm{MeV}/c^2$ pole of the $\eta\eta$–S–wave to $\eta\eta'$ does not improve the fit. The results remain stable (fit #2, #5, #7).

- Next it was tried to improve the fit by introducing the $a_2(1320)$ which although at the phase space limit could contribute due to its finite width. In fit #9 the mass and width of the $a_2(1320)$ were fixed to the PDG values. This improves the fit in comparison to #6: χ^2=2185/(1798-27)=1.23. Both 2^{++} resonances were allowed to annihilate from S and P initial states. The $a_2(1320)$ contributes with 2.8%. Releasing mass and width of the $a_2(1320)$ improves the fit insignificantly and shifts the $a_2(1320)$ mass far out of phase space.

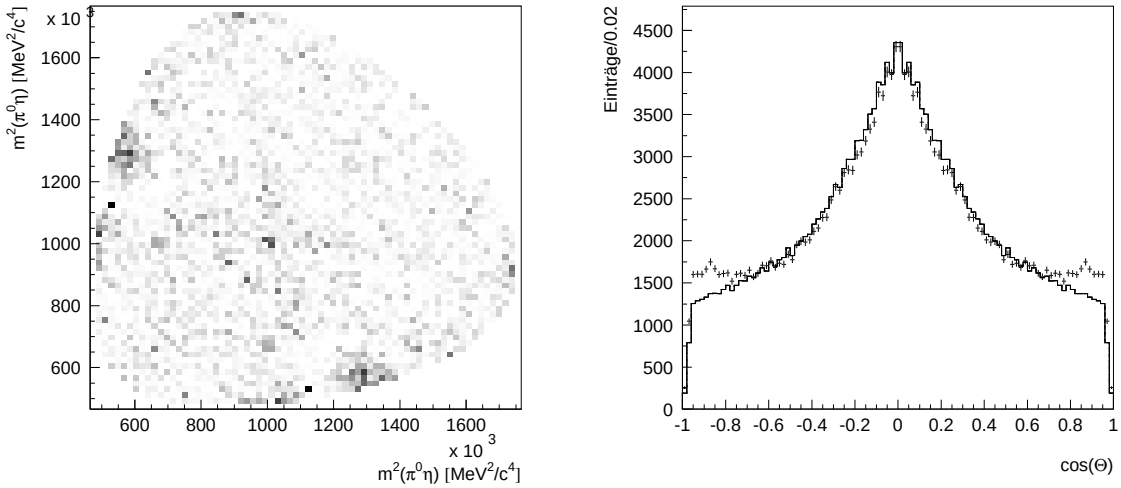

Figure 7.1: *The necessity of introducing a tensor resonance in $\eta\eta$. The left hand figure shows the χ^2 distribution of fit #6 without a 2^{++} resonance and the right figure the angular distribution in $\eta\eta$ between 1465 MeV/c^2 and 1565 MeV/c^2*

Fit#		$\pi^0\eta$–S–wave		$\eta\eta$–S–wave			$\eta\eta$–D–wave	$\pi^0\eta$–D–wave
		Pole 1	Pole 2	Pole 1	Pole 2	Pole 3	Pole 1	Pole 1
1	$\|\beta\|$	0.13	–	0.22	0.35	2167	0.24	–
	$\arg(\beta)$	–	–	-2.92	9.25	8.13	16.38	–
2	$\|\beta\|$	0.13	–	0.22	0.35	1455	0.24	–
	$\arg(\beta)$	–	–	-2.91	9.26	8.12	16.38	–
3	$\|\beta\|$	0.20	0.39	0.09	0.16	–	0.10	–
	$\arg(\beta)$	–	-0.08	-4.66	8.75	–	18.34	–
4	$\|\beta\|$	0.16	0.39	0.13	0.21	718.5	0.10	–
	$\arg(\beta)$	–	0.64	-4.13	8.84	7.04	18.72	–
5	$\|\beta\|$	0.16	0.40	0.13	0.21	726.0	0.10	–
	$\arg(\beta)$	–	0.63	-4.13	8.84	7.04	18.73	–
6	$\|\beta\|$	0.19	1.32	0.18	0.22	1290	0.13	–
	$\arg(\beta)$	–	2.44	-4.59	8.09	6.49	18.16	–
7	$\|\beta\|$	0.19	1.32	0.18	0.22	1351	0.13	–
	$\arg(\beta)$	–	2.44	-4.59	8.09	6.49	18.16	–
8	$\|\beta\|$	0.13	–	0.21	0.34	2373	0.20	0.14
	$\arg(\beta)$	–	–	-2.89	9.34	8.16	16.51	14.74
9	$\|\beta\|$	0.14	0.79	0.16	0.29	1017	0.15	0.14
	$\arg(\beta)$	–	2.09	-4.10	8.50	7.04	15.77	2.07
10	$\|\beta\|$	0.17	1.39	0.21	0.29	1390	0.09	–
	$\arg(\beta)$	–	2.56	-4.55	8.35	6.54	18.59	–

Table 7.3: *Production strength of the fitted hyotheses for the* $^1S_0$ *initial state.*

Fit #	$f_0(1400)$		$f_0(1500)$		f_2	
	$m[\mathrm{MeV}/c^2]$	$\Gamma[\mathrm{MeV}/c^2]$	$m[\mathrm{MeV}/c^2]$	$\Gamma[\mathrm{MeV}/c^2]$	$m[\mathrm{MeV}/c^2]$	$\Gamma[\mathrm{MeV}/c^2]$
1	1392	223	1511	128	1498	151
2	1393	223	1512	136	1498	152
3	1317	378	1497	106	1518	73
4	1366	210	1509	120	1523	65
5	1366	210	1509	120	1523	65
6	1328	214	1485	80	1547	113
7	1323	220	1485	64	1547	113
8	1406	208	1524	134	1498	151
9	1393	288	1499	136	1547	113
10	1356	206	1510	122	1525	48

Table 7.4: *T–matrix–parameters of the* $\eta\eta$*–resonances*

Fit #	$f_0(1400)$ [%]	$f_0(1500)$ [%]	high mass [%]	f_2 [%]	$\pi^0\eta$–S–wave [%]
1	20.9	30.6	8.4	34.0	6.1
2	21.6	29.6	8.6	34.0	6.1
3	5.5	8.0	–	0.5	86.0
4	10.4	13.8	3.5	0.5	71.8
5	11.9	11.9	3.9	0.5	71.8
6	13.8	9.4	7.2	15.4	54.2
7	13.9	9.6	6.9	15.4	54.2
8	19.6	27.6	12.3	30.9	6.6
9	14.5	25.9	3.6	20.2	32.8
10	18.5	18.5	8.8	0.2	54.0

Table 7.5: *Contribution of the resonances to the $\pi^0\eta\eta$ final state*

	mass [MeV/c^2]	width [MeV/c^2]	BR
$f_0(1400)$	1360 ± 35	245 ± 60	$(3.2 \pm 1.6) \cdot 10^{-4}$
$f_0(1500)$	1505 ± 15	115 ± 30	$(3.8 \pm 2.2) \cdot 10^{-4}$
f_2	1530 ± 15	110 ± 60	$(2.9 \pm 2.9) \cdot 10^{-4}$

Table 7.6: *Final $\eta\eta$–resonance parameters. The error includes the statistics as well as the systematic uncertainties.*

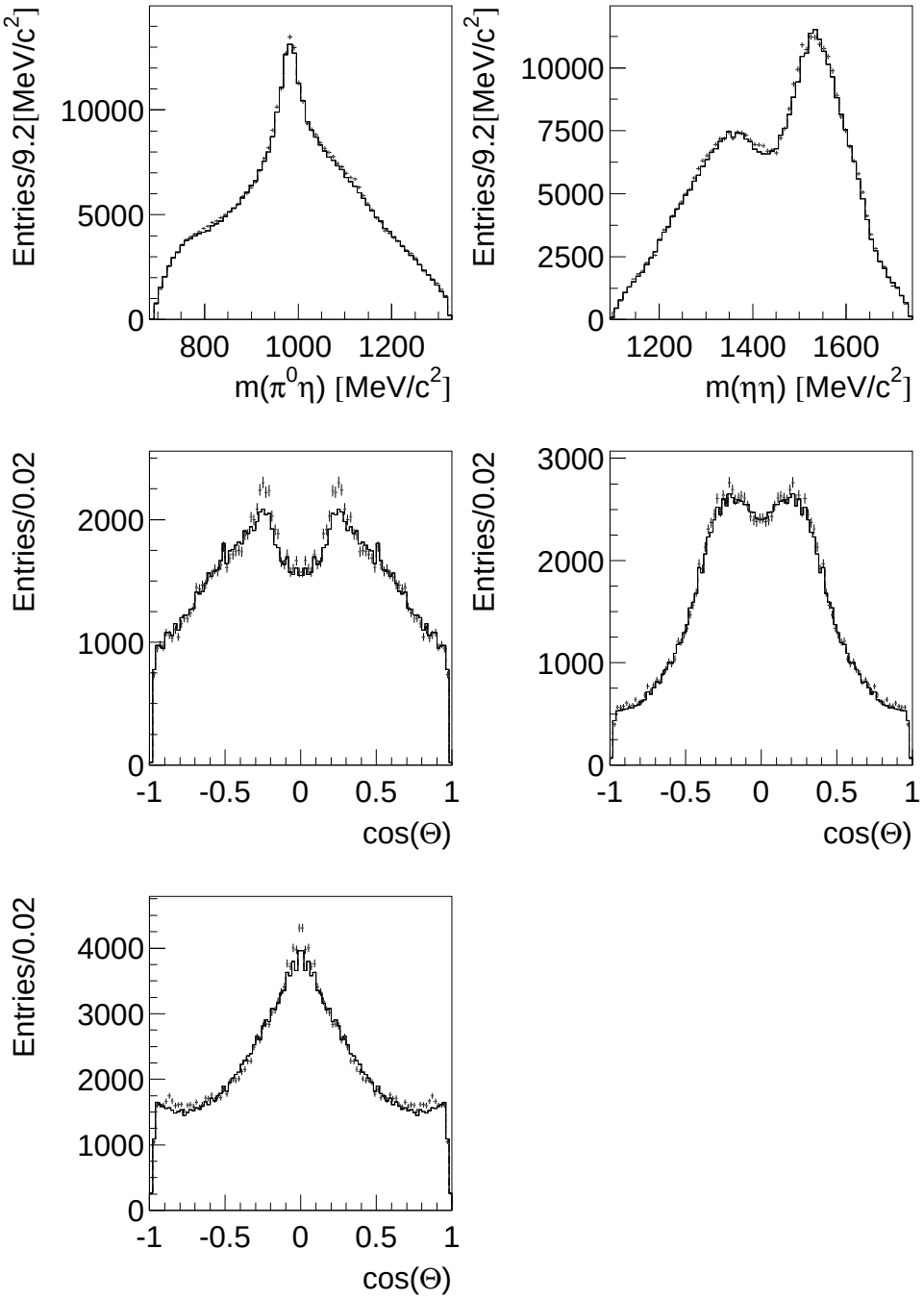

Figure 7.2: *Fitresult #1. $\pi^0\eta$ projection, $\eta\eta$ projection, angular distribution in $\pi^0\eta$:* $(980 \pm 30)\,MeV/c^2$. *Angular distribution in $\eta\eta$:*$(1400 \pm 50)\,MeV/c^2$ *and* $(1515 \pm 50)\,MeV/c^2$.

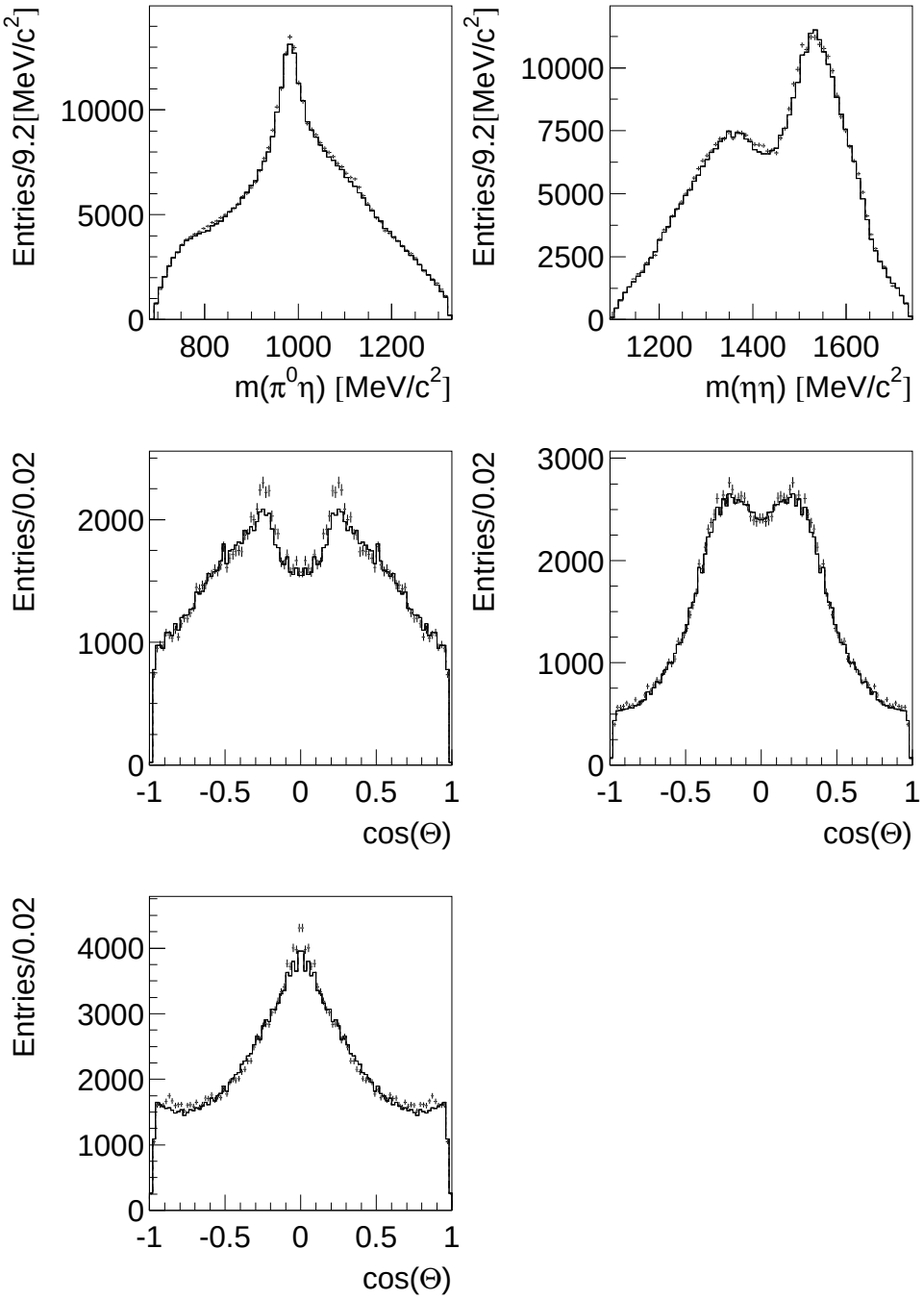

Figure 7.3: *Fitresult #2. $\pi^0\eta$ projection, $\eta\eta$ projection, angular distribution in $\pi^0\eta$:* $(980 \pm 30)\,MeV/c^2$. *Angular distribution in $\eta\eta$:*$(1400 \pm 50)\,MeV/c^2$ *and* $(1515 \pm 50)\,MeV/c^2$.

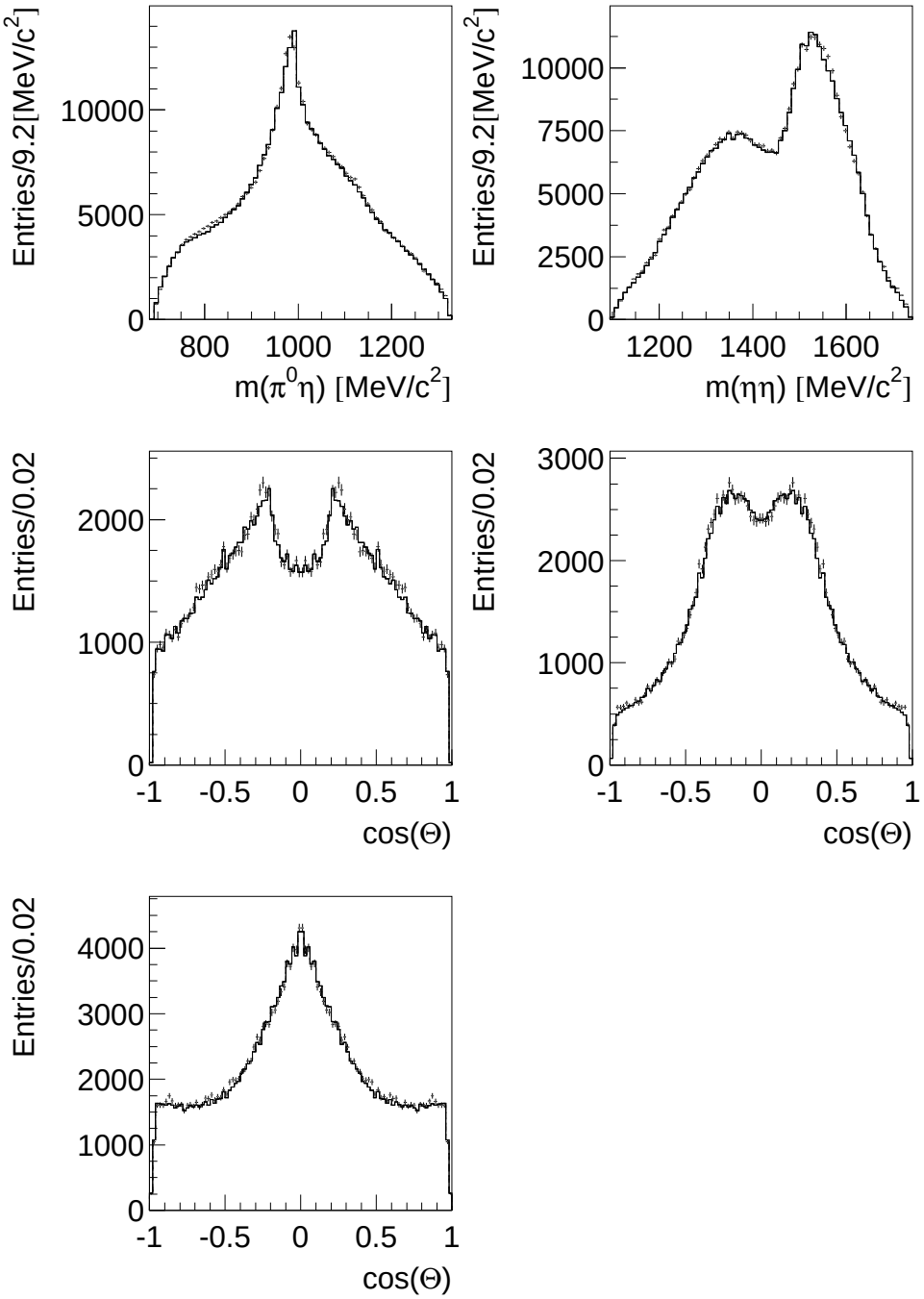

Figure 7.4: *Fitresult #3. $\pi^0\eta$ projection, $\eta\eta$ projection, angular distribution in $\pi^0\eta$:* $(980 \pm 30)\ MeV/c^2$. *Angular distribution in $\eta\eta$:*$(1400 \pm 50)\ MeV/c^2$ *and* $(1515 \pm 50)\ MeV/c^2$.

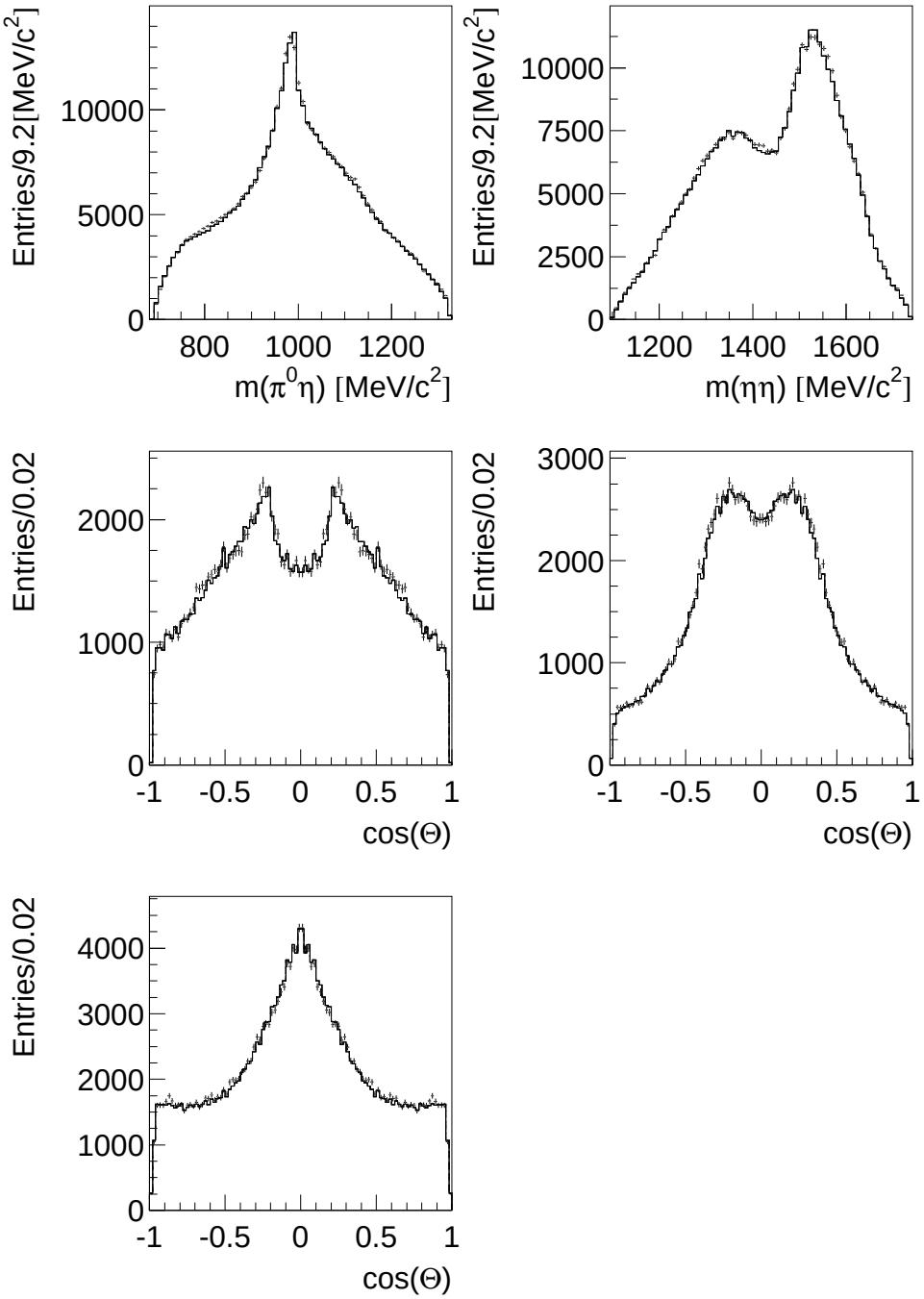

Figure 7.5: *Fitresult #4. $\pi^0\eta$ projection, $\eta\eta$ projection, angular distribution in $\pi^0\eta$:* $(980 \pm 30)\,MeV/c^2$. *Angular distribution in $\eta\eta$:*$(1400 \pm 50)\,MeV/c^2$ *and* $(1515 \pm 50)\,MeV/c^2$.

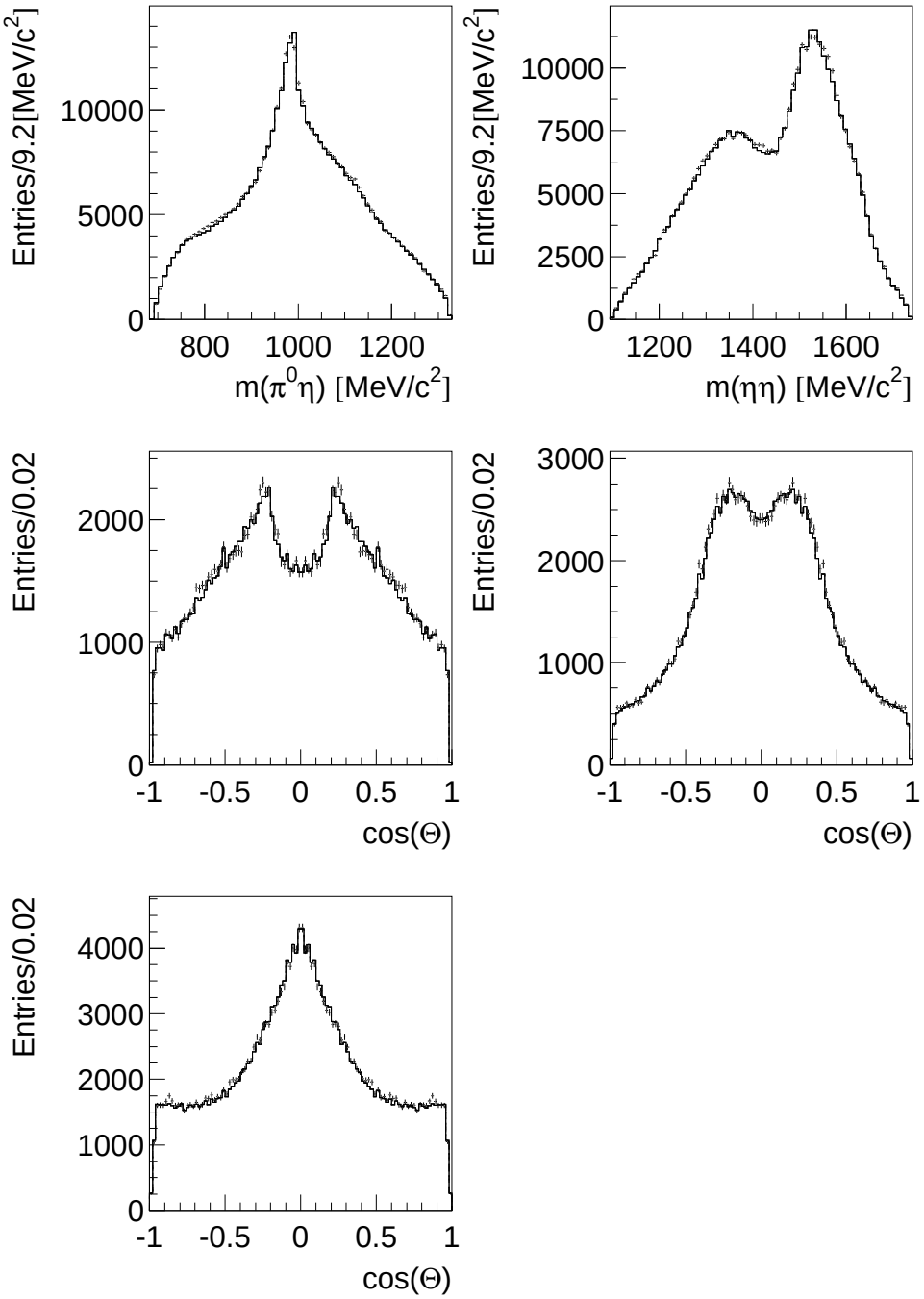

Figure 7.6: *Fitresult #5. $\pi^0\eta$ projection, $\eta\eta$ projection, angular distribution in $\pi^0\eta$:* $(980 \pm 30)\,MeV\!/c^2$. *Angular distribution in $\eta\eta$:*$(1400 \pm 50)\,MeV\!/c^2$ *and* $(1515 \pm 50)\,MeV\!/c^2$.

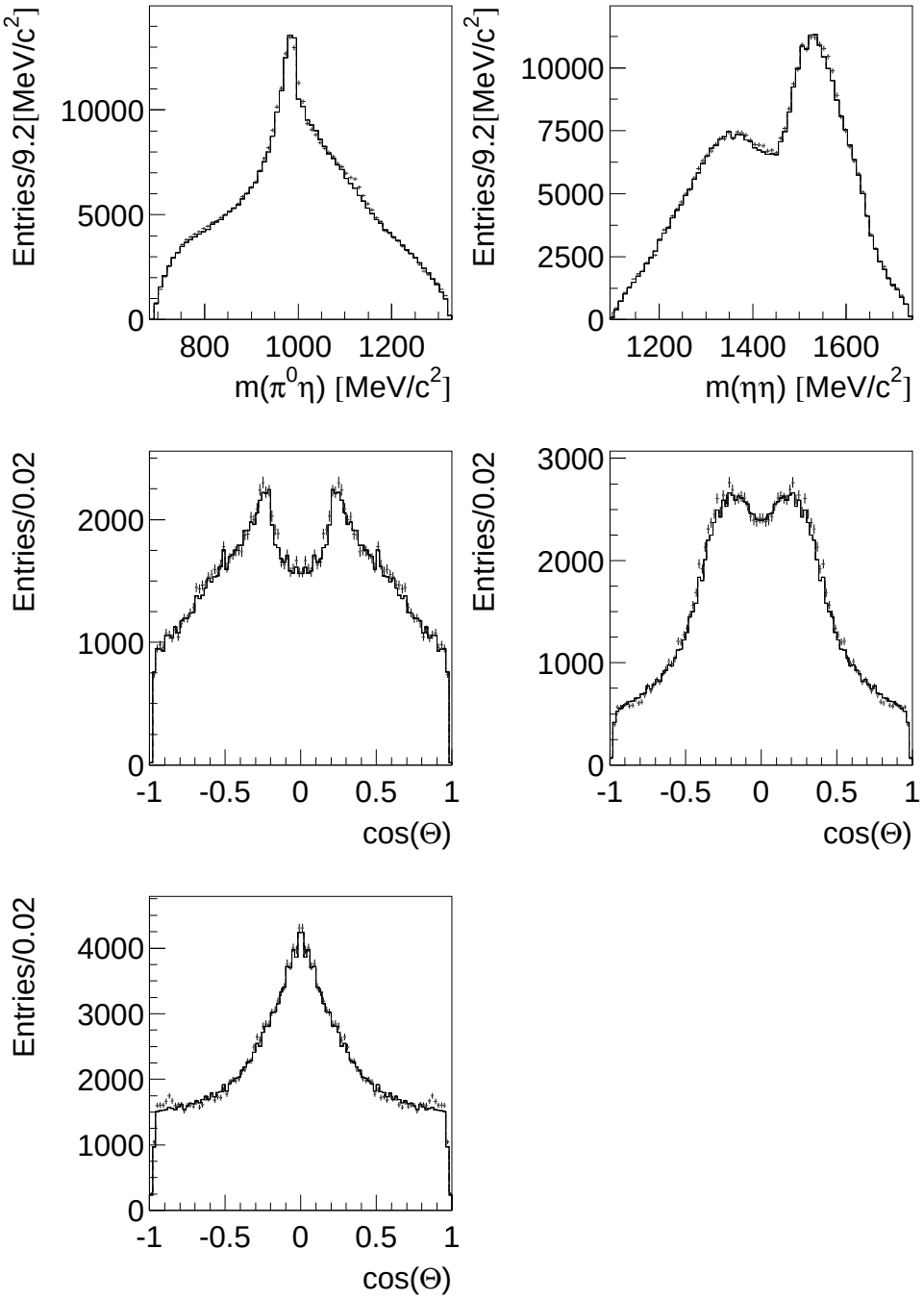

Figure 7.7: *Fitresult #6.* $\pi^0\eta$ *projection,* $\eta\eta$ *projection, angular distribution in* $\pi^0\eta$*:* $(980 \pm 30)\,MeV\!/c^2$*. Angular distribution in* $\eta\eta$*:*$(1400 \pm 50)\,MeV\!/c^2$ *and* $(1515 \pm 50)\,MeV\!/c^2$*.*

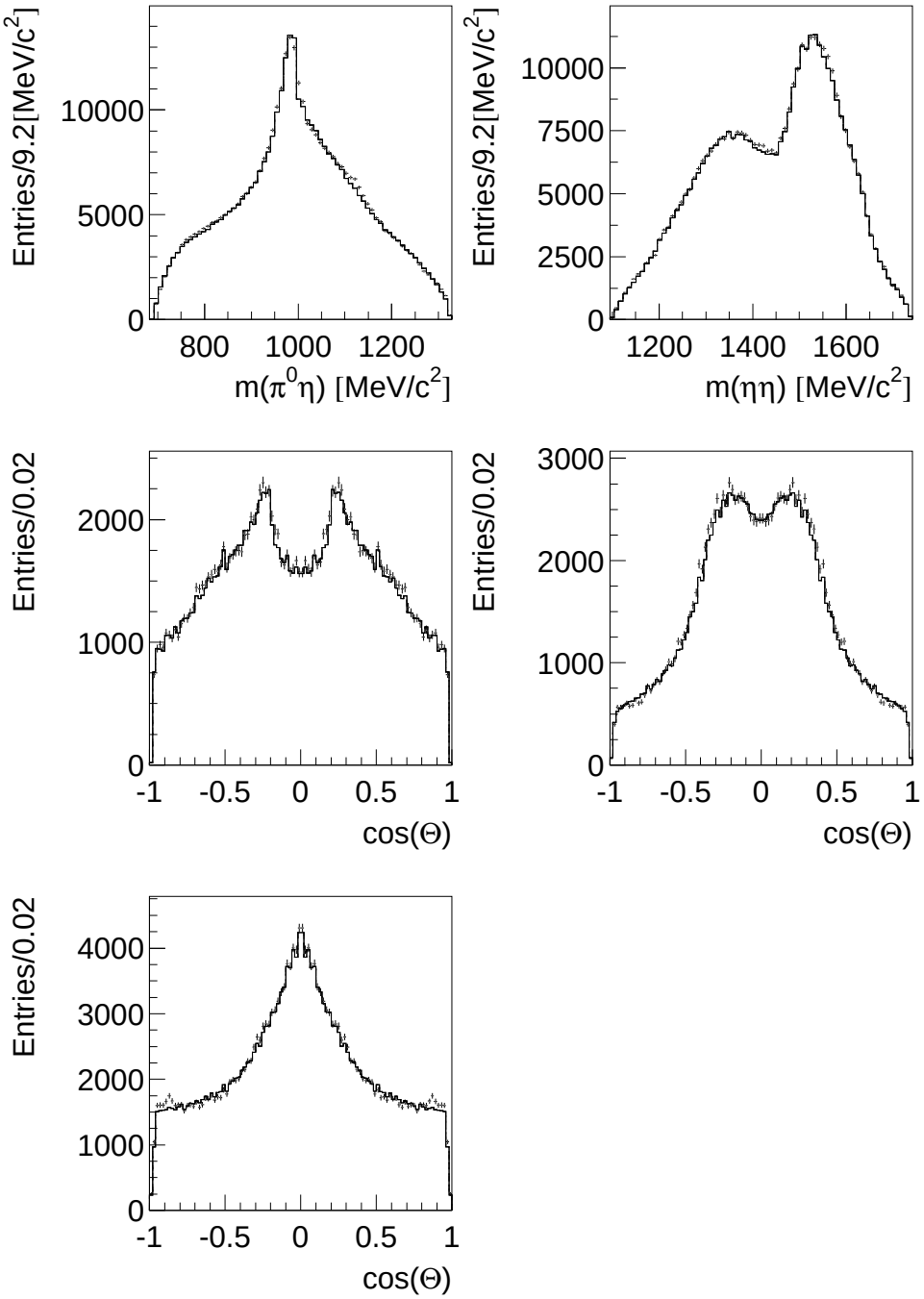

Figure 7.8: *Fitresult #7. $\pi^0\eta$ projection, $\eta\eta$ projection, angular distribution in $\pi^0\eta$:* $(980 \pm 30)\,MeV/c^2$. *Angular distribution in $\eta\eta$:*$(1400 \pm 50)\,MeV/c^2$ *and* $(1515 \pm 50)\,MeV/c^2$.

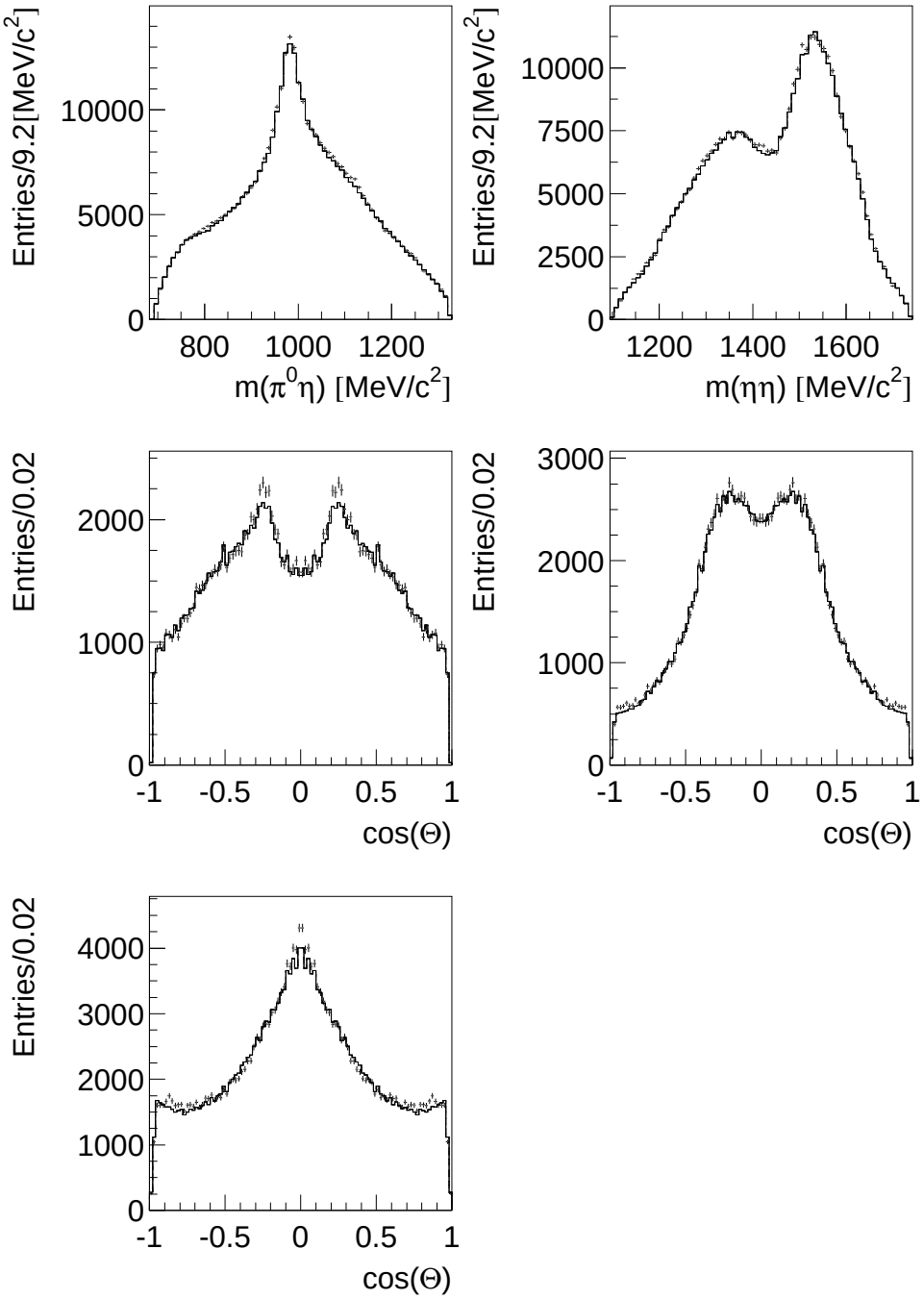

Figure 7.9: *Fitresult #8. $\pi^0\eta$ projection, $\eta\eta$ projection, angular distribution in $\pi^0\eta$:* $(980 \pm 30)\ MeV/c^2$. *Angular distribution in $\eta\eta$:*$(1400 \pm 50)\ MeV/c^2$ *and* $(1515 \pm 50)\ MeV/c^2$.

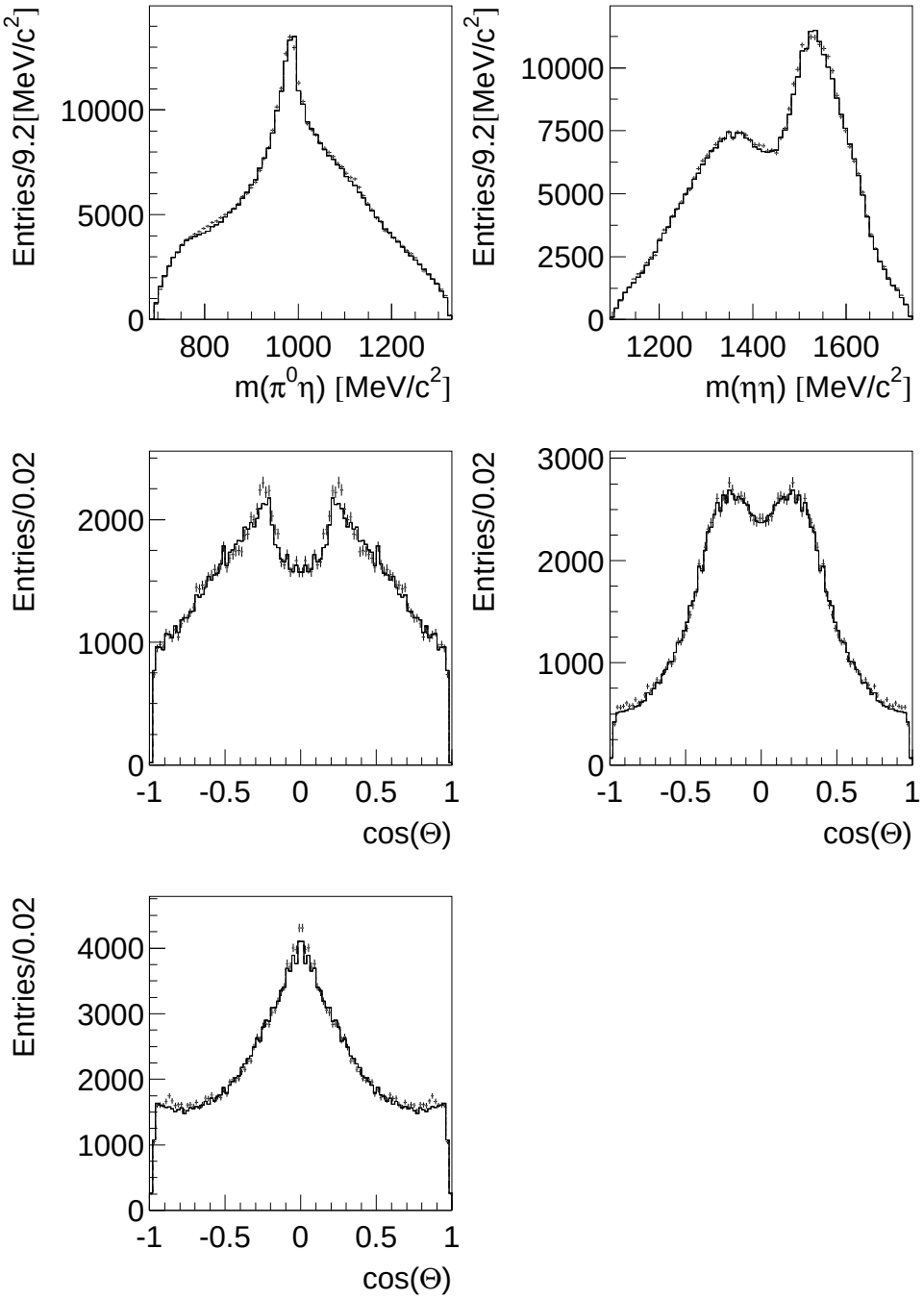

Figure 7.10: *Fitresult #9.* $\pi^0\eta$ *projection,* $\eta\eta$ *projection, angular distribution in* $\pi^0\eta$*:* $(980 \pm 30)\,MeV\!/c^2$*. Angular distribution in* $\eta\eta$*:*$(1400 \pm 50)\,MeV\!/c^2$ *and* $(1515 \pm 50)\,MeV\!/c^2$*.*

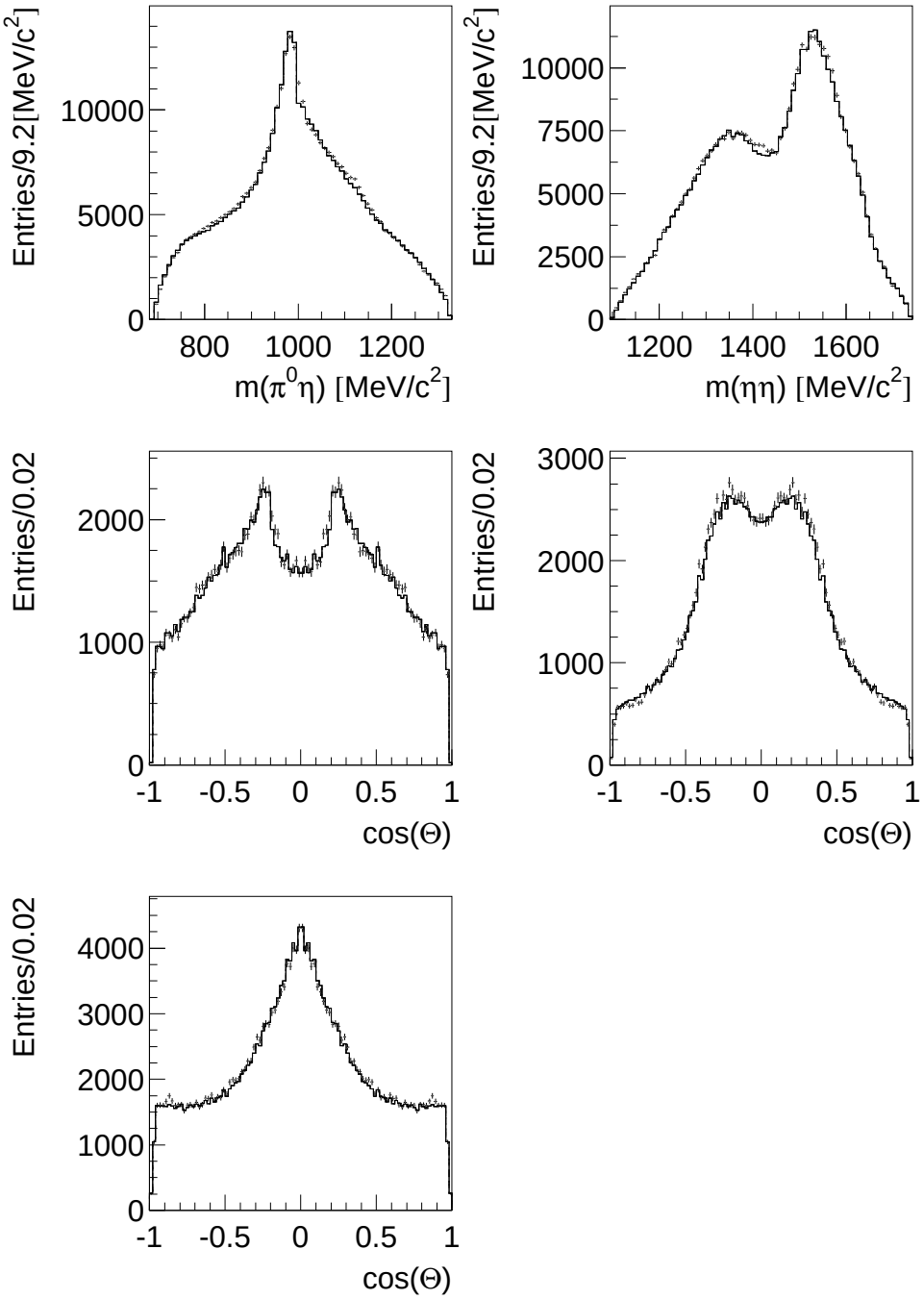

Figure 7.11: *Fitresult #10.* $\pi^0\eta$ *projection,* $\eta\eta$ *projection, angular distribution in* $\pi^0\eta$*:* $(980 \pm 30)\,MeV\!/c^2$*. Angular distribution in* $\eta\eta$*:*$(1400 \pm 50)\,MeV\!/c^2$ *and* $(1515 \pm 50)\,MeV\!/c^2$*.*

Appendix A

Further fits

In addition to the fits described above some fits were made where a 4.5% flat background was subtracted from the data. These fits were:

1. $\pi\eta$–S–wave: 2 poles fixed, free β
   $\pi\eta$–D-wave: 1 pole fixed at PDG–values ($a_2(1320)$)
   $\eta\eta$–S–wave: 2 poles (1×1–K–matrix with one channel
   $\eta\eta$–D–wave: one Breit–Wigner amplitude (free mass and width)

2. $\pi\eta$–S–wave: 2 poles fixed, free β
   $\pi\eta$–D-wave: 1 pole fixed at PDG–values ($a_2(1320)$)
   $\eta\eta$–S–wave: 2 poles (1×1–K–matrix with one channel
   $\eta\eta$–D–wave: 2 Breit–Wigner amplitudes with $f_2(1270)$ fixed at PDG values

3. $\pi\eta$–S–wave: 1 pole free, free β
   $\pi\eta$–D-wave: 1 pole fixed at PDG–values ($a_2(1320)$)
   $\eta\eta$–S–wave: 2 poles (1×1–K–matrix with one channel
   $\eta\eta$–D–wave: one Breit–Wigner amplitude (free mass and width)

4. $\pi\eta$–S–wave: 2 poles fixed, free β
   $\pi\eta$–D-wave: 1 pole fixed at PDG–values ($a_2(1320)$)
   $\eta\eta$–S–wave: 3 poles (1×1–K–matrix with one channel
   $\eta\eta$–D–wave: one Breit–Wigner amplitude (free mass and width)

All fits were done using the $\pi^0\eta\eta$–Dalitz plot with a 4.5% flat background subtraction. The projections of these fits look rather well, but the T–matrix parameters of the resonances are not as one would naively expect. This problem is linked to the fact that only two poles in the $\eta\eta$–S–wave were used. Fit #1 is the same as the best fit, but only two poles in the $\eta\eta$–S–wave instead of 3 poles. In fit#2 the description of the $\eta\eta$–D-wave is done by the introduction of two Breit–Wigner amplitudes. This violates unitarity but has the advantage that it is easy to fix mass and width to the PDG–values. So this fit is something like a *hybrid* analysis. In fit #3 the $\pi\eta$–S-wave was parametrized as a K–matrix with one pole only coupling to 2 channels ($\pi\eta$ and $\mathrm{K\bar{K}}$). The parameters (mass and width) of the $a_0(980)$ are not reasonable The fit finds the following K–matrix parameters for the $a_0(980)$ $m = 995.4, \widetilde{\Gamma}_{\pi\eta} = 505.8, \widetilde{\Gamma}_{\mathrm{K\bar{K}}} = 12.5$.

As given in table 0.5 the contribution of the $\pi\eta$–S–wave increases when leaving the poles free. Further the contribution of the $\eta\eta$–S–wave is too small. When I fixed the $\pi\eta$–S–wave poles the contribution of the $\eta\eta$–S–wave increased. I should mention that the evaluation of the contribution to the Dalitzplot of the $\eta\eta$–S–wave resonances is a numerical approximation, because it neglects interference effects.

The third pole in the $\eta\eta$–S–wave stabelizes the fit. It weakens the influence of the resonance parameters on the different hypotheses. In addition the width of the $f_0(1400)$ is then smaller ($\approx 300\,\mathrm{MeV}$ instead of $\approx 600\,\mathrm{MeV}$).

#	$a_0(980)$ $^1S_0$			$\eta\eta$–S–wave $^1S_0$				$\eta\eta$–2^{++}–BW		$a_2(1320)$ fix	χ^2/N_{dof}	P/S
	BW	$\pi^0\eta$–S–wave fix	$\pi^0\eta$–S–wave free	1×1	2×2 $\eta\eta/\eta\eta'$	2 Poles	3 Poles	$^1S_0$	S+P	S+P		
1		x		x		x			x	x	1.36	0.14
2		x		x		x			x	x	1.31	0.27
3			x	x		x			x	x	1.44	0.13
4		x		x			x		x	x	1.31	0.19

Table A.1: *The table gives the hypotheses tried to fit the data.*

Fit–#	$\eta\eta$–S–wave poles								
	m_1	$\widetilde{\Gamma}_{11}$	$\widetilde{\Gamma}_{12}$	m_2	$\widetilde{\Gamma}_{21}$	$\widetilde{\Gamma}_{22}$	m_3	$\widetilde{\Gamma}_{31}$	$\widetilde{\Gamma}_{32}$
1	1353	301	–	1612	341	–	–	–	–
2	1341	323	–	1594	295	–	–	–	–
3	1362	185	–	1565	161	–	–	–	–
4	1350	217	–	1569	217	–	$1.3\cdot 10^5$	21	–

Table A.2: *The K–matrix poles of $\eta\eta$–S–wave*

Fit#		$\pi^0\eta$–S–wave		$\eta\eta$–S–wave			$\eta\eta$–D–wave		$\pi^0\eta$–D–wave
		Pole 1	Pole 2	Pole 1	Pole 2	Pole 3	Pole 1	Pole 2	Pole 1
1	$\|\beta\|$	0.15	0.93	0.14	0.26	–	0.12	–	0.18
	arg(β)	–	2.00	-4.30	8.91	–	15.9	–	2.12
2	$\|\beta\|$	0.15	0.84	0.15	0.26	–	0.16	0.03	0.14
	arg(β)	–	2.05	-4.22	8.71	–	15.8	20.6	102.7
3	$\|\beta\|$	0.17	–	0.04	0.14	–	0.13	–	0.09
	arg(β)	–	–	-3.83	8.95	–	17.19	–	5.52
4	$\|\beta\|$	0.15	0.82	0.15	0.28	877.6	0.15	–	0.14
	arg(β)	–	2.07	-4.13	8.50	7.00	15.78	–	2.08

Table A.3: *Production strength of the fitted hyotheses for the $^1S_0$ initial state.*

Fit #	$f_0(1400)$		$f_0(1500)$		f_2	
	m[MeV/c^2]	Γ[MeV/c^2]	m[MeV/c^2]	Γ[MeV/c^2]	m[MeV/c^2]	Γ[MeV/c^2]
1	1433	616	1487	124	1497	210
2	1391	606	1494	114	1492	118
3	1393	232	1512	130	1524	161
4	1391	298	1501	136	1494	155

Table A.4: *T–matrix–parameters of the $\eta\eta$–resonances*

	Fit	1 [%]	2 [%]	3 [%]	4 [%]
$^1S_0$	$a_0(980)$	38.6	32.0	77.7	35.4
	$a_2(1320)$	1.4	0.7	0.3	0.82
	$f_2(1270)$		0.3	–	–
	f_2	2.3	2.2	1.8	3.0
	$f_0(1400)$	15.0	14.5	0.85	12.5
	$f_0(1500)$	28.8	23.9	7.2	26.1
	high mass	–	–	–	2.7
$^3P_1$	$a_2(1320)$	2.8	1.4	0.45	0.45
	$f_2(1270)$	–	0.9	–	–
	f_2	3.9	5.3	0.3	6.2
$^3P_2$	$a_2(1320)$	3.7	1.8	0.1	1.4
	$f_2(1270)$	–	2.0	–	–
	f_2	5.9	15.3	12.5	11.4
Σ		100.0	100.3	101.2	100.0

Table A.5: *Contribution of the resonances to the $\pi^0\eta\eta$ final state*

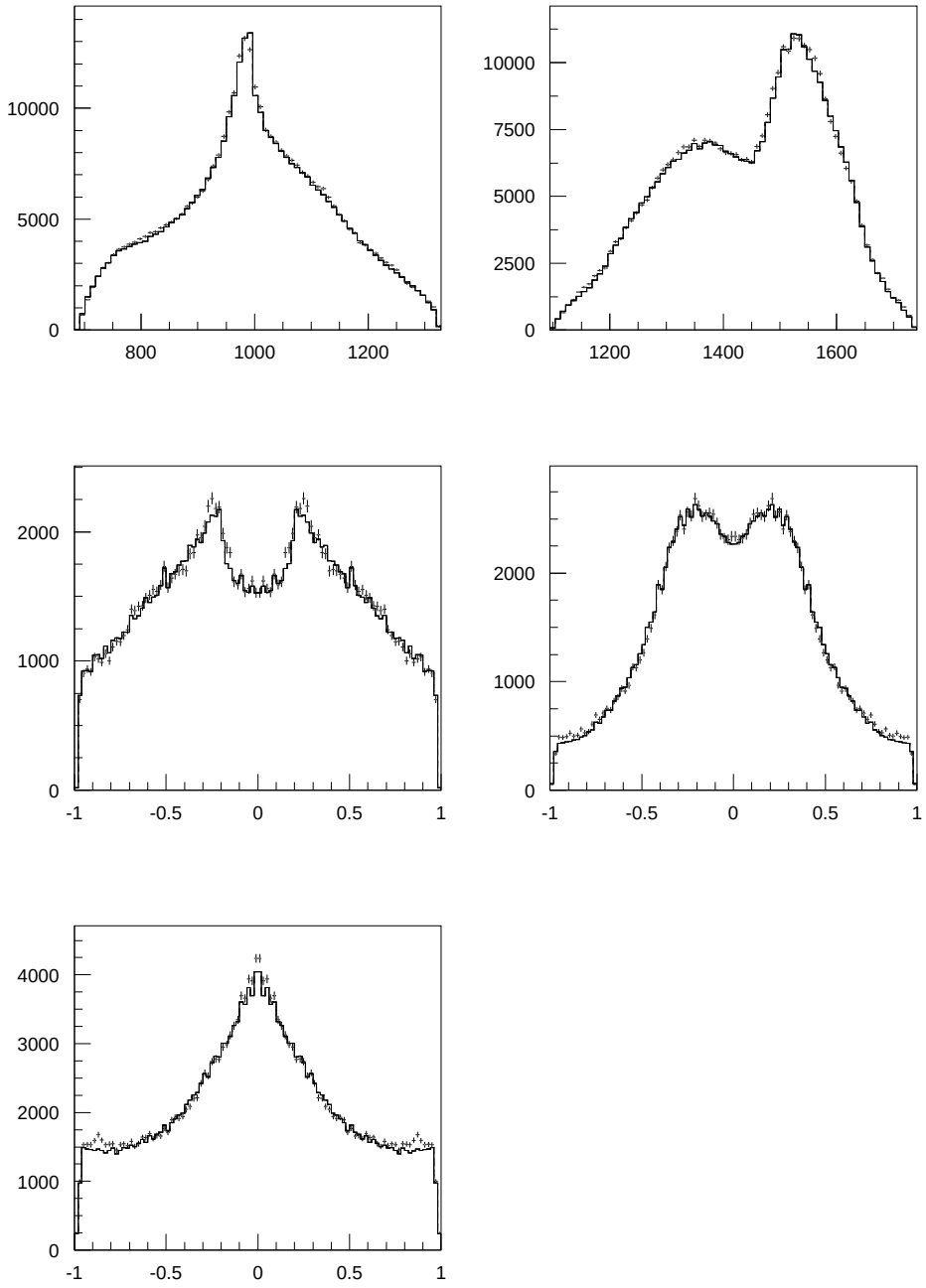

Figure A.1: *Fitresult #1.* $\pi^0\eta$ *projection,* $\eta\eta$ *projection, angular distribution in* $\pi^0\eta$*:* $(980 \pm 30)\,MeV\!/c^2$*. Angular distribution in* $\eta\eta$*:*$(1400 \pm 50)\,MeV\!/c^2$ *and* $(1515 \pm 50)\,MeV\!/c^2$*.*

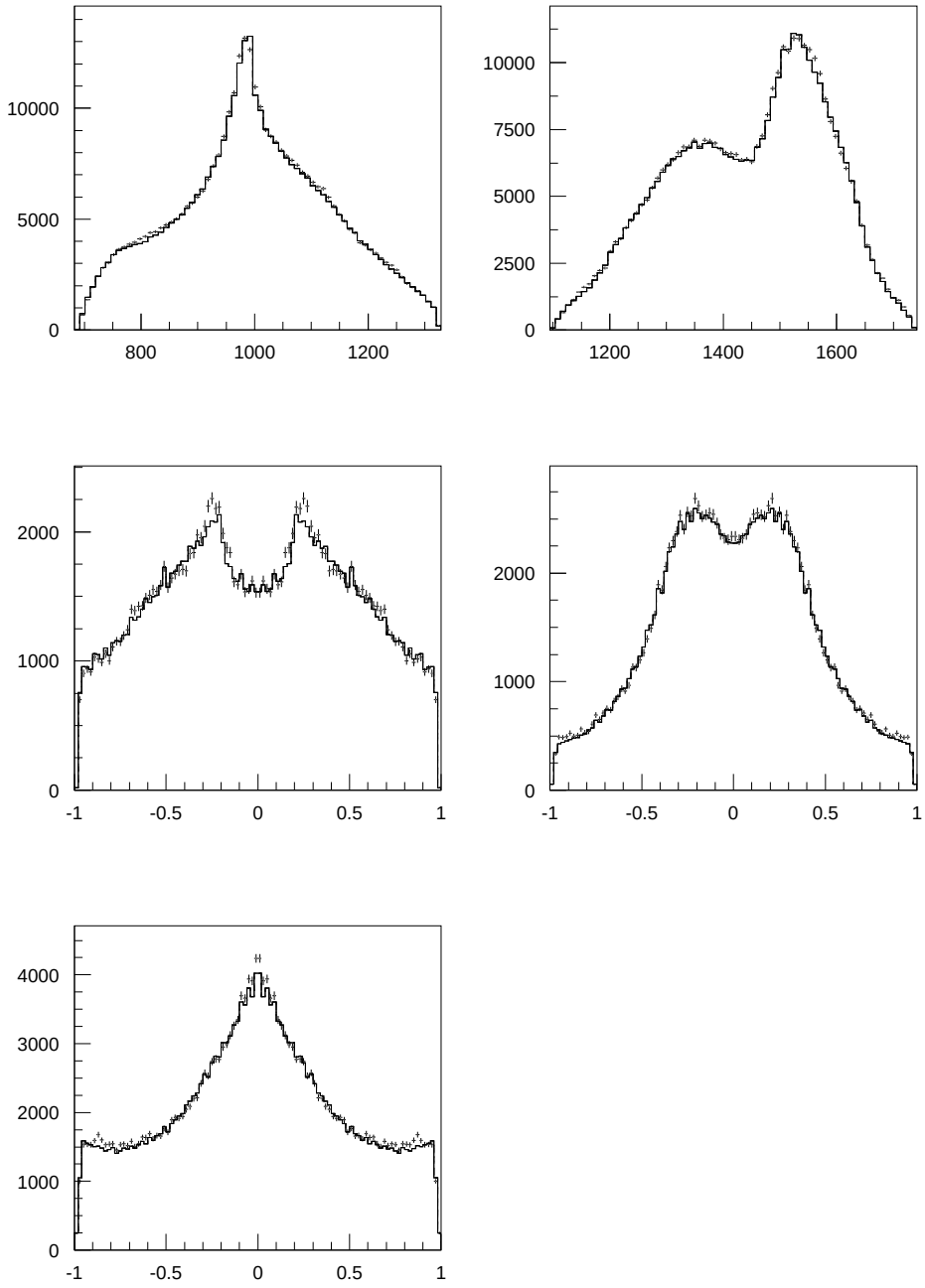

Figure A.2: *Fitresult #2.* $\pi^0\eta$ *projection,* $\eta\eta$ *projection, angular distribution in* $\pi^0\eta$*:* $(980 \pm 30)\,MeV\!/c^2$*. Angular distribution in* $\eta\eta$*:*$(1400 \pm 50)\,MeV\!/c^2$ *and* $(1515 \pm 50)\,MeV\!/c^2$.

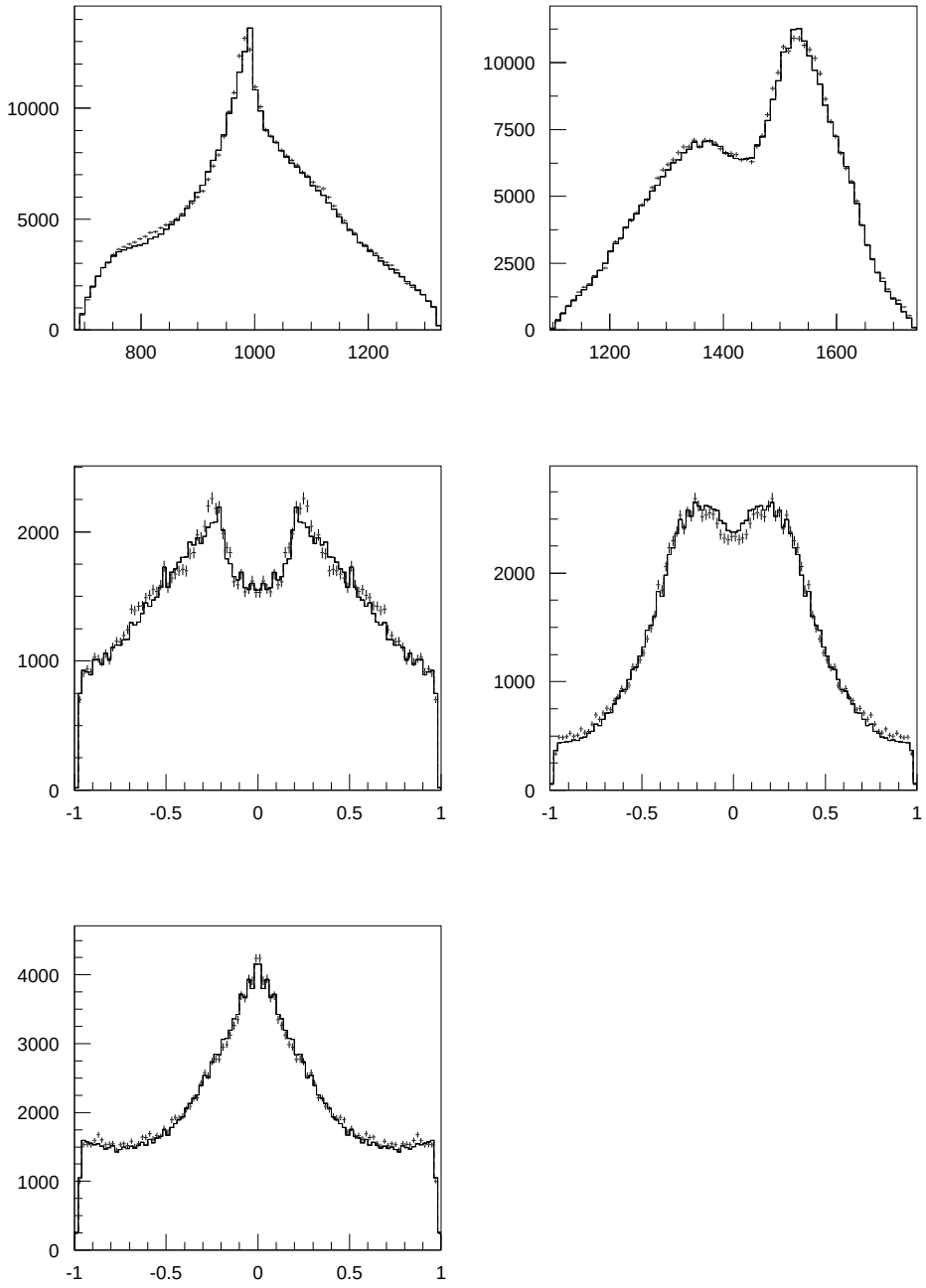

Figure A.3: *Fitresult #3.* $\pi^0\eta$ *projection,* $\eta\eta$ *projection, angular distribution in* $\pi^0\eta$*:* $(980 \pm 30)\,MeV\!/c^2$*. Angular distribution in* $\eta\eta$*:*$(1400 \pm 50)\,MeV\!/c^2$ *and* $(1515 \pm 50)\,MeV\!/c^2$.

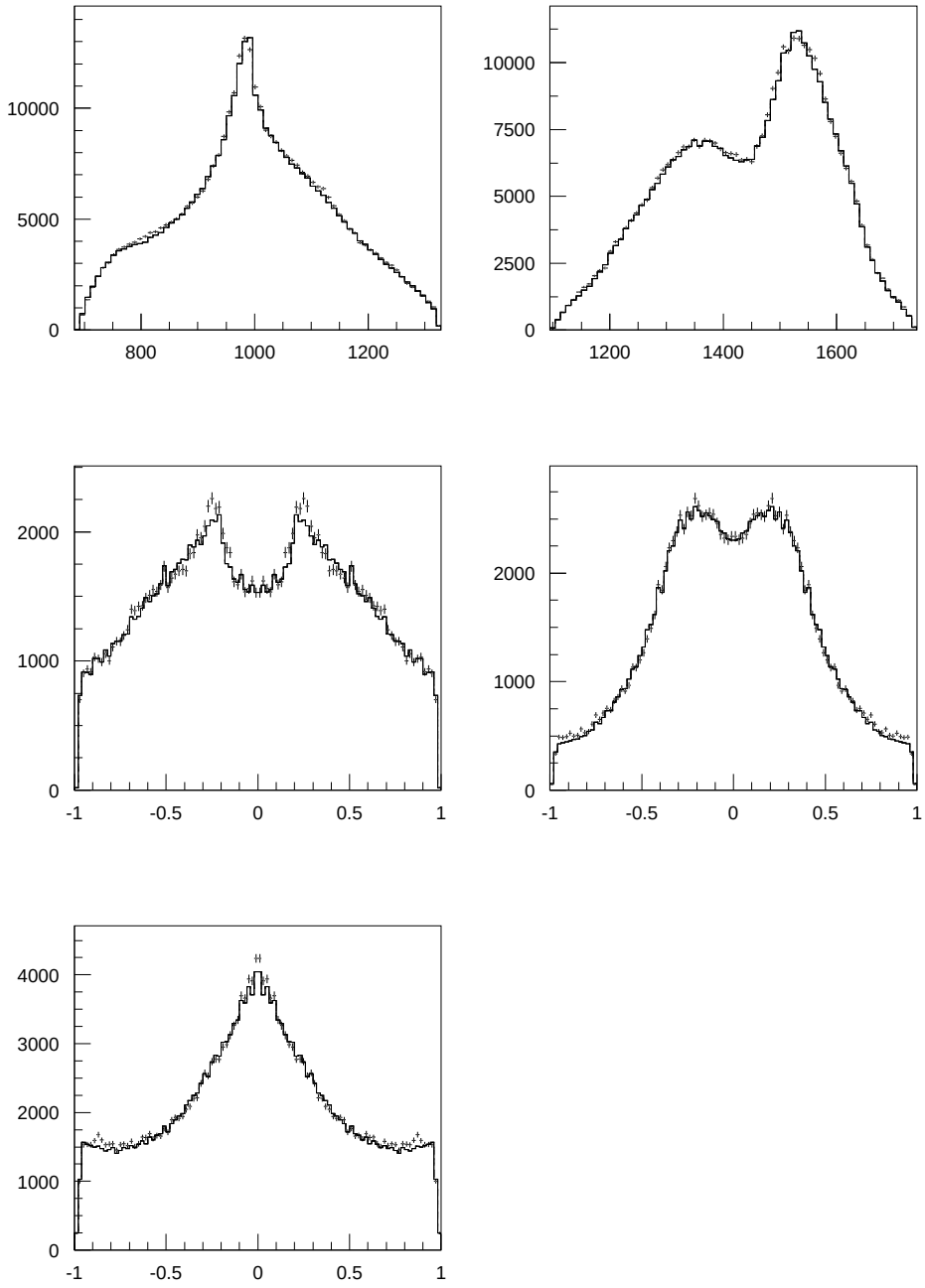

Figure A.4: *Fitresult #4. $\pi^0\eta$ projection, $\eta\eta$ projection, angular distribution in $\pi^0\eta$:* $(980 \pm 30)\,MeV\!/c^2$. *Angular distribution in $\eta\eta$:*$(1400 \pm 50)\,MeV\!/c^2$ *and* $(1515 \pm 50)\,MeV\!/c^2$.